Ezersky *Geo-Engineering (2017)8:13*
DOI 10.1186/s40703-017-0050-2

International Journal of Geo-Engineering

ORIGINAL RESEARCH Open Access

Behavior of seismic-acoustic parameters during deforming and failure of rock samples, large blocks and underground opening: base for monitoring

M. G. Ezersky*

*Correspondence:
mikhail@geotec.co.il
Geotec Engineering and Environmental Geophysics Ltd, P.O.B. 25031, 7502501 Rishon Lezion, Israel

Abstract

Construction of engineered projects, such as underground spaces, tunnels, machine halls etc. is connected with variations in stress-state and deformations of large volumes of rock mass. Latter can results in damage of rocks, their collapse into underground space, danger for equipment and risk for human life. To avoid such consequences different in situ geotechnical and geophysical monitoring is carried out during construction and exploitation of underground structures. Geophysical monitoring is based on observations for behavior of elastic shear- and longitudinal wave velocities (Vs and Vp, respectively) and microseismic activity. Behavior of the elastic velocities during deforming of the rock depends on type of the future failure that, in turn, is defined by structure and properties of medium and characteristics of stress state σ_3/σ_1 and hydrostatic pressure. These velocity variations are defined by difference in effective parameters of forming microfractures, whose geometry is distinguished at different modes of stress-state. At that character of interaction between microfractures determines type of the macrofailure. We studied behavior of longitudinal wave velocities during loading of rock samples, large blocks and underground opening orienting measurements along maximum (σ_1) and minimum (σ_3) stresses. It is shown that velocity variations along maximum stress is more informative at elastic phase of rock deformations (velocity increases), whereas velocity variations along axis of minimum stress is more informative at the stage of nonlinear deformation of rock (velocity begin decrease). These regularities are well appeared at deforming of large blocks and unloading of rock mass in underground openings. This knowledge should be used at planning and performing of monitoring of stability of underground structures.

Keywords: P- and S-wave velocity, Rock failure, Stress-state, Ultrasound, Underground hall

Introduction

The construction and exploitation of the largest hydro underground complexes at seismic tectonically active regions is resulted in intensive deformation processes at the shallow subsurface, which could be reason of the serious accidents [1–5]. Apart from this, creation of underground opening within stressed rock mass modifies their stress state [6, 7]. Therefore, the construction of the underground complexes with extended tunnels of

tens kilometer long and more than 10 m diameters, machine halls of the 50–60 m height and some hundred meters long, and highest concrete dams of some hundreds meter height have required the carrying out monitoring of their stability during construction works [8]. Such monitoring based on geophysical parameters using seismic geotomography, ultrasonic and acoustic emission methods have carried out during construction of the high concrete dam Inguri hydro power station (HPS) [9], large underground opening [10–14] and tunnels [15, 16, 4]. A monitoring is based on exact knowledge of the regularity of geophysical parameters behavior at all stages of the rock deformation process including this just before its failure. The influence of scale effect on acoustic parameters in rocks was also studied [8, 17].

The present work was performed with an aim to study the behavior of the elastic velocities and acoustic emission inside the zones of the forming of both shear and tensile macro fractures during loading to failure of the rock samples and large blocks. The longitudinal velocity (Vp) behavior is discussed.

The numerous studies on rock samples have shown that failure of the polycrystalline medium such as rocks is not instant process. It follows in time and is prepared by accumulation and interaction of the microfractures which result the rupture or shear macrofracture forming [18]. The variations of the physics-mechanics rock properties preceding to the failure allows using the different geophysical methods sensitive to such variations with an objective to predict the failure. It first is related to seismic-acoustic methods based on monitoring of the different waves spreading in the deformed medium, their velocity and attenuation (closely connected with the microfractures parameters) measurement [19, 20] and acoustic emission observation [21, 12, 22]. In spite of the high level of the modern loading machines and laboratory test equipment for samples testing, it is necessary to study the large volume of the rock in situ. It permits to avoid influence of the sample boundaries and loading machines stiffness influence as well as to study differentially the failure development in the space.

Failure model

The failure in the strict sense is failure surfaces forming [23]. Muller defines three main rupture modes: rupture by separation, rupture by sliding and rupture by shearing. Studying the rock samples failure Hoek [24] names the first rupture mode as tensile failure (Fig. 1) and two last rupture modes as shear failure (shear).

At that the tensile fracture is oriented perpendicularly to the minimum normal stress axis σ_3 ($\alpha_S = 0^o$) and shear rupture is oriented by angles between 0° and 45° to σ_1 (the compression is regarded as positive and $\sigma_1 > \sigma_2 > \sigma_3$). The rupture surfaces formed as the failure result we will name macrofracture. The microfractures is a discontinuity formed from initial defects as a stress acting result. It is experimentally proved that at the elastic–plastic and plastic rock behavior its failure takes place as result of microfractures accumulation, grouping and their interaction at the stresses closed to the strength limit. The avalanche like failure stage takes place at the critical microfractures density followed by the macrofracture forming [21, 25].

Stavrogin and Protosenya [26] have proposed universal model of the heterogeneous media shear failure based on numerous experimental data acquired at the wide range of the stress state mode. The model explains the dilatancy phenomenon characteristic

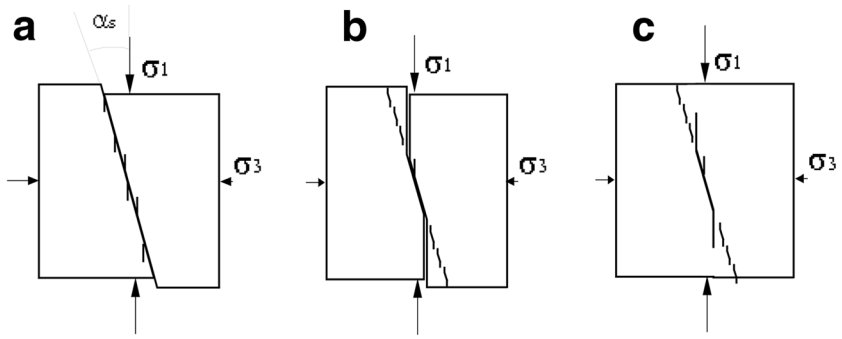

Fig. 1 Suggested rupture modes under compressive stress conditions. **a** Shear failure; **b** Tensile failure; **c** Stable crack configuration (by Hoek [24])

for all rocks. Analyzing the experimental data authors make the conclusion that it is not possible to explain residual deformations of rock using only the shear deforming mechanism. The presumable deforming and failure scheme in isotropic heterogeneous material is represented lower (Fig. 2).

At the failure of the rock sample deformed by the major normal stress σ_1 and $\sigma_2 = \sigma_3$ macroscopic shear plane ω is formed inclined to the rock axis by angle of α_S (named "failure angle"). It follows from experimental data that the failure angle increases and it is approached to 40°–45° as stress state mode $C = \sigma_3/\sigma_1$ ratio increases. The shear

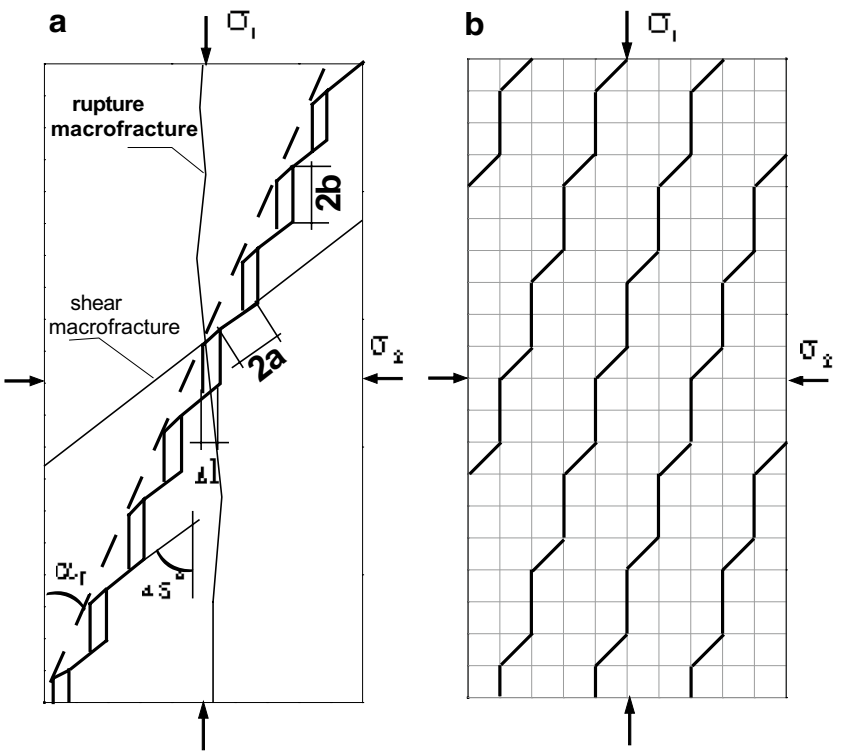

Fig. 2 Model of the shear failure by Stavrogin and Protosenya [26]: shear macrofracture (**a**) and failure micro-elements (**b**)

macrofracture is represented as combination of the shear and failure microplanes (elements). The shear microplanes are inclined by angle of 45° to compression axis (they are inter-grained defects, in first approaching). The tensile microelements are oriented along the compression axis and they can be considered as a microfractures growing from shear element tips like mechanism described by Hoek (Fig. 1). The external stresses results shear along 2a element and tensile on 2b one (Fig. 2). Then failure angle α_s will be depending on a and b inter-relation. At the case, a = b failure angle $\alpha_s = 22.5°$. The parameter $\chi = b/a$ is entered:

$$\chi = 0.707 * \left(\mathrm{Ctg}\,\alpha_s - 1\right) \quad (1)$$

Parameter χ determines the inclination angle of the failure macro plane ω to main compression axis and, in its turn, it is determined by the stress state mode $C = \sigma_3/\sigma_1$.

It follows from expression (1) at the $\alpha_S = 45°$ parameter $\chi = 0$ and material is deformed along shear planes coinciding with a plane of maximum shear stress (sliding). At the failure angle $\alpha_S = 0°$ parameter $\chi = \propto$ and macrofracture is pure tensile crack oriented along compression axis. At the intermediate case (α_S is between 0° and 45°) the macrofracture is combination of shear and tensile and shear failure takes place. In reality to get the failure angles of 45° in rocks is practically impossible because of rock heterogeneity (it is very difficult even in soils, especially coarse and medium grained).

The above described model shows one and the same the rupture origin and universal mechanism could be considered in its frames.

Model of the solid with numerous fractures

For description of the dilatancy and failure stages the models of the solid with numerous fractures are used [27, 20]. The loaded rock is represented as a homogeneous isotropic or transversal-isotropic solid (or matrix) with elastic modulus Em (or velocity Vm) including the numerous statistically distributed isolated fractures whose concentration uniquely defines the effective elastic characters of the medium E or V. The fracture filling has effective elastic parameters Ef or Vf. The fractures it is supposed are circle in plane and they have radius a. The fractures have cross-section of the elliptical shape with the half axises of b and a size as it is shown in Fig. 3a. The α = b/a ratio is named the aspect ratio (or shape coefficient). The fracture concentration parameter is defined as $\upsilon = N^*a^3$, where N is the fractures number within single volume (fracture density). The relative effective elastic modulus E/Em versus fractures concentration υ for isotropic and transversal-isotropic medium [20] are represented in Fig. 3a.

One of the important consequences of this model is that E/Em parameter (which slightly depend on Poisson's ratio) is a measure of the fracture concentration. The other important consequence is obtained if to connect the velocity variation with a fracture volume. The relative velocity V/Vm versus fractures volume n% is represented in Fig. 3b.

It can see that velocity dependence on both fracture volume and fracture shape takes place. At the same fractures volume, the long narrow fractures (the aspect ratio is low: α = 0.001, for instance) results the more considerable velocity decrease than short or sphere similar fractures (pores) with a high aspect ratio of 0.1–1.0. At the same aspect ratio, the velocity decrease is measure of the fractures volume. Because nonlinear dependence mode the history of the fracture accumulation takes place. The loading of

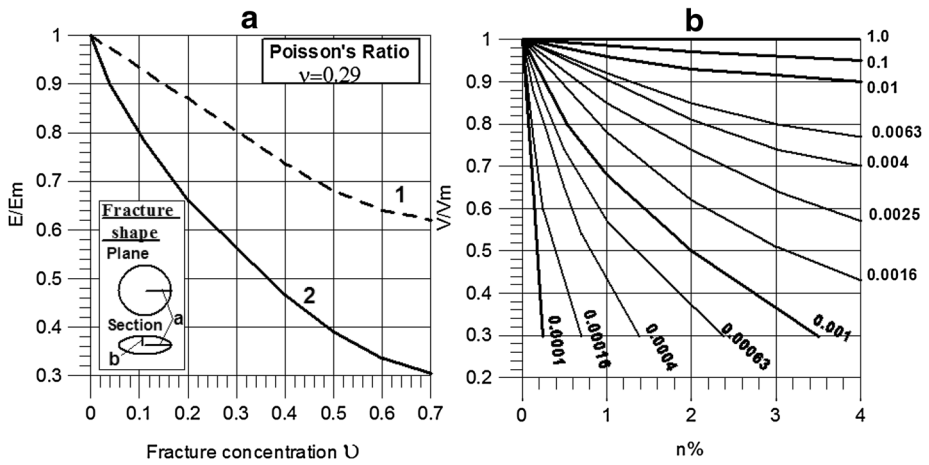

Fig. 3 Model of the solid with numerous fractures. **a** Inter-relations between fractures concentration (υ) and relative velocity (V/Vm) for isotropic (*1*) and transversal isotropic (*2*) mediums; **b** Inter-relations between fractures summary volume (n%) and relative velocity (V/Vm). *Curves parameter* is the aspect ratio α = b/a

the rock volume results an inelastic volumetric deformation (dilatancy) which is the fracture volume variation [28]. So, measuring velocity variations versus inelastic volumetric deformation ε_v (or ε_3 axial inelastic deformation) somewhat information about the modal fractures aspect ratio values could be obtained.

Methods

Ultrasonic measurements on samples under uniaxial pressure

Loading conditions

Rock sample (1 in Fig. 4a) was placed to the loading machine (2 in Fig. 4a). Then a sample was loaded by small steps from zero to load destructing sample. At every load level, different parameters were measured (deformations, velocities of P- and S-waves, acoustic emission (Fig. 4a).

Different destruction modes were determined by conditions on contact of machine with end faces of samples. Number of samples were tested in the still cell with sand. In this cell, the sample was in a volumetric stress–strain state at uniaxial loading. To get

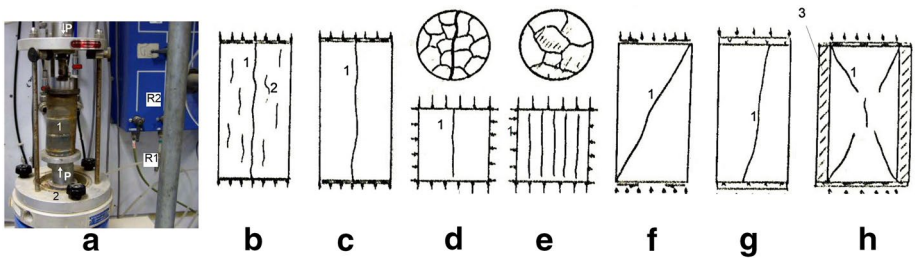

Fig. 4 Loading machine (**a**) and types of the macrofractures in destructed samples. **b**, **c** Rupture of I and II modes, respectively; **d**, **e** Rupture of mode III in basalt and limestone, respectively, obtained at the triaxial loading in the cell with sand; **f**–**h** shear macrofracture, obtained at loading with dry friction, with cardboard gaskets and with grease on contact with the end faces of the sample. In (**b**–**h**) *1* macrofracture, *2* concurrent fractures, *3* still cell

numerous rupture fractures, end faces of samples were smeared with petroleum jelly etc. The types of macrofracture destructed a sample are shown in Fig. 4b–h.

Ultrasonic measurements

The ultrasonic measurements were carried out for calculations of the pulse velocities of compression waves (Vp) and shear waves (Vs) in rock samples and the determination of ultrasonic elastic constants of an isotropic rock, or one exhibiting slight anisotropy [29]. The velocity measurement procedure was carried out in accordance with ASTM D2845 [30]. The primary advantages of ultrasonic testing are that it yields compression and shear wave velocities, and ultrasonic values for the elastic constants of intact homogeneous isotropic rock specimens.

Apparatus

For laboratory measurements, we used the S-70 device (1 in Fig. 5b) that is the compact field ultrasonic meter (hereafter, US-meter) with photographic signal registration by the Institute of the Physics of Earth, Russian Academy, [31].

Photographic registration of the signal is carried out using a digital camera mounted on a special tube (2 in Fig. 5b). For laboratory measurements transducers of 100 kHz were used. The US-meter comprises the time-mark quartz generator that provides highly accurate arrival time readings of not less than 0.1–0.2 μs (6 in Fig. 5c). The absolute accuracy of Vp determination, with respect to intact rock (Vp = 5500 m/s), at a sample length of 70 mm is of 0.8–1.2%. During US measurements arrival times are measured (4 and 5 in Fig. 5c). Velocities of elastic waves (Vp and Vs) are calculated using a simple formula V = l/t, were l is the length of sample and t is arrival time.

Photographic registration of the signal is carried out using a digital camera mounted on a special tube. Both time marks and signal were recorded simultaneously. A switch box allows for switching P- and S-transducers without disconnecting them from the device. P-wave records (4 in Fig. 5c) are characterized by sharp arrivals. Shear-wave records are identified in accordance with Rao and Lakshmi [32] as a sharp arrival on a

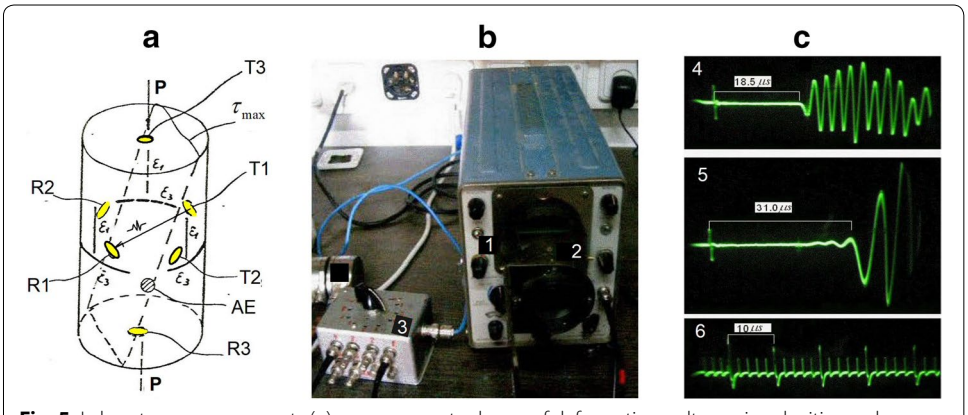

Fig. 5 Laboratory measurements (**a**) measurement schema of deformations, ultrasonic velocities and acoustic emission: T—US transmitter and R—receivers with their numbers, ε_{1-3}—different components of deformations, *AE* acoustic emission; *P* axial load; **b** US-meter S-70 (*1*) with photographic registration of signal (*2*) and switch of channels (*3*); **c** Ultrasonic records obtained on samples: *4* P-wave records, *5* S-wave records, *6* time marks (there are 2 μs between minor marks)

background of forerunner P-wave light oscillations (5 in Fig. 5c). In a number of cases, verification of shear waves was carried out by rotating the shear wave transducer (changing the polarization direction from horizontal to perpendicular) and checking the corresponding variation in a wave phase.

Ultrasonic logging

Ultrasonic profiling in boreholes is aimed to measure the distribution of Vp and Vs with depth.

Method and equipment

In ultrasonic logging (USL) the elastic waves spreading from a high frequency (50–70 kHz) transmitter to receivers along the borehole wall under investigation [33]. Savich et al. [34] suggested "dotty" (detailed) ultrasonic logging for enabling measuring elastic velocities within 0.1–0.2 m distance along the borehole walls. Since the probe is held against the side of the wall, the results are unaffected by the "adjacent beds" effect (as it is in seismic refractions) because of the wave's direct path. Wave penetration into the rock is approximately 0.1–0.2 m in accordance with the wave length. The US-meter is intended mainly for ultrasonic measurements in boreholes using special multi-channel probe.

The schema of the dotted ultrasonic logging is shown in Fig. 6a–c.

In our investigation, a 7-transducer probe (developed by Hydroproject Institute, Moscow, Russia), with a 0.1 m separation between sensors (Fig. 6c), was placed into the borehole (Fig. 6a) and clamped onto the wall by means of a pneumatic camera pumped by air from the surface or metallic clamps. It provided excellent contact between the probe and the borehole wall. Every transducer (made of 70 kHz frequency piezoelectric ceramic) can act both as transmitter (T) and as receiver (R) when connected to a generator or oscilloscope. Switching is carried out with a switch-box (3 in Figs. 5b, 6b). Elastic wave spreading along the borehole wall from transmitter arrives consequently to the receiving

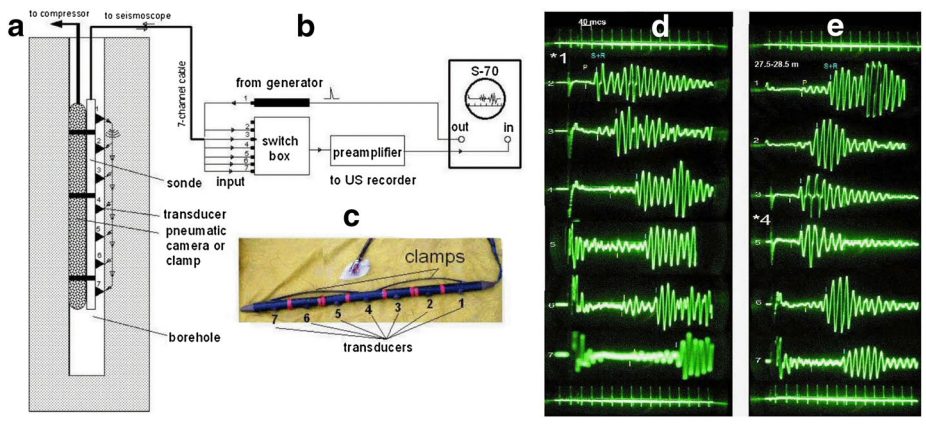

Fig. 6 Borehole logging lay-outs. **a** Ultrasonic logging: 7-transducer probe within the boreholes; **b** communication schema; **c** probe photography; **d**, **e** Ultrasonic records obtained during ultrasonic logging in the borehole (digits denote numbers of transducers): **d** 1st transducer is transmitter; 2nd–7th transducers are receivers (direct shot); **e** 4th transducer is transmitter, the 1st–3rd and 5th–7th ones are receivers (split shot). P and S+R (interference shear and surface waves) arrivals are marked by *yellow* and *white*, respectively

sensors where it is converted, gained, and visualized on the oscilloscope's electronic tube of the US-meter S-70 (Fig. 6b) that was described above.

There is also the moment of wave triggering (start of transmission) on the tube (see Fig. 6d). The time difference (t) between triggering time and signal arrival at the nth receiver is the spread-time between transmitter and receiver along a fixed distance equal to the $l = (n-1) \times 0.1$ m (the separation) between neighboring sensors. The wave velocity is then defined by simply dividing: $V = l/t$. Examples of field records are presented in Fig. 6d, e. The transmitting transducer in Fig. 6d is no.1 marked on records by an asterisk (see ultrasonic probe in Fig. 6c for explanation). Figure 6e shows records of ultrasonic pulses received at receivers 2 through 6. Arrival times of P-waves are denoted by yellow vertical markers. Arrival times of S + R waves are marked by green vertical markers. In Fig. 6e, the schema of shot (named split) has been shown: the transmitter is transducer no. 4 and receiving transducers are 1-st–3rd and 5th–7th. Physically, arrival times are calculated using a time scale (from above and from below the records). The time scale between two marks in Fig. 6d, e is 40 μs.

The velocity behavior during the rock samples deforming

The above mentioned have shown that it is possible to study the different kind failures in frame of the universal shear failure model using the velocity measurements based technique. The main regularities of the velocity behavior during the failure forming will be considered in this chapter (here and later we discuss the longitudinal velocities behavior having in view that the similar behavior of the shear wave velocities have to take place). The whole rock samples volume is considered whose deformations and velocity variation at the different loads and in different directions are measured. It is known [3, 35] that there are the characteristic deformation stages during the rock deforming according to the different loading level which is acting effective stress T divided by the ultimate (maximum) one Tm (Fig. 7a). They are: stage of inelastic deformation connected with a fracture closing (I), quasi elastic linear behavior (II), inelastic deformation (dilatancy stage III) connected with a microfractures opening and development and, at last, failure stage (IV) which includes the microfractures interaction and macrofracture forming destroying the deformed volume. Ezersky [28] has established that inelastic volumetric deformation (dilatancy) dependents on the failure mode: tensile failure is appeared in small deformations, whereas shear one results the great deformations.

In accordance with deformation rock behavior the velocities are varied also. The waves spreading along the normal maximum stress σ_1 (named also axial velocities, V'') (Fig. 7b) and waves spreading along σ_3 direction ($V^{\perp}$ in Fig. 7c) shows the different behavior. At the stage I and II V'' increases in more degree than $V^{\perp}$, whereas at the dilatancy (III) and failure (IV) stages it is contrary: as a load increases $V^{\perp}$ decreases always whereas V'' either does not vary or varies considerably slighter than $V^{\perp}$.

The quasi anisotropy in velocity variation (Fig. 7d) is appeared, which can reach 80–90% at the rupture failure forming and it can be of 20–40% during the shear failure forming. The different behavior of the $V^{\perp}$ takes place preceding to different failure mode: velocity decrease for tensile failure starts at the lower stress level ($\sigma/\sigma_s = 0.1$–0.2) than it takes place for shear macrofracture forming ($\sigma/\sigma_s = 0.6$–0.7). As a rule, in samples destroyed by the tensile fracture the maximum velocity decrease (to 50% of

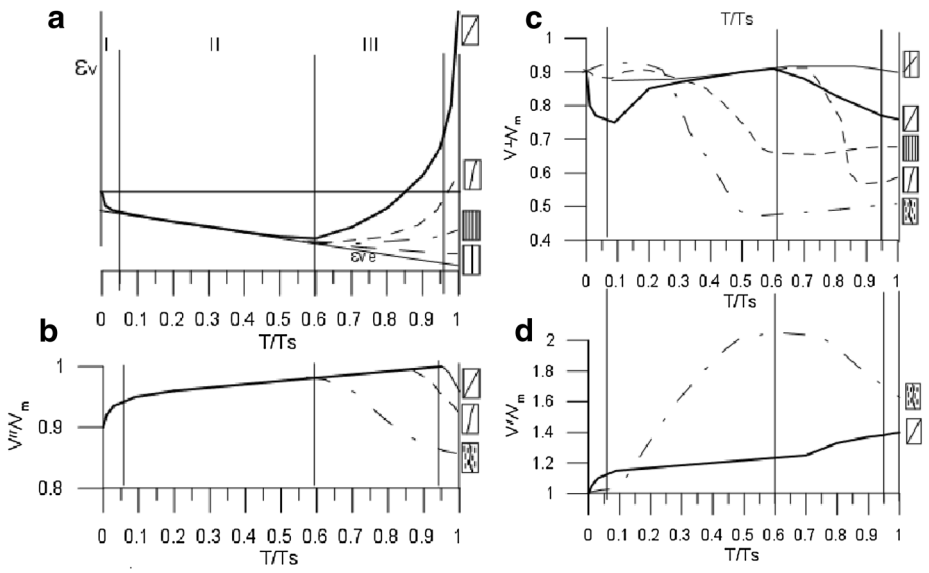

Fig. 7 Generalized behavior of the deformations and velocities during the sample loading (pictures are the sample macrofracture mode). **a** characteristic deformation stages; **b** variation with stress level of $V''/V''m$ (relative axial velocity spreading along the normal maximum stress σ_1; **c** variation with stress level of $V^{\perp}/V^{\perp}m$ (e.g. relative axial velocity spreading along the normal minimum stress σ_3; **d** variation with stress level of $V^{\perp}/V''$. Pictures in *right* of graphs shows mode of sample failure

maximum value) is reached at the low and medium stress level ($\sigma/\sigma_s = 0.2$–0.5), whereas for shear macrofracture forming it takes place at the high stress level ($\sigma/\sigma_s = 0.7$–0.9). The velocity decrease in case of shear failure is smaller (to 20% of maximum value).

Above considered failure model in connection with the Salganik model [20] permitted interpreting of the velocity behavior in samples during their loading to failure. The velocities $V^{\perp}$ behavior is explained by variation of the axial (tensile) microfractures concentration. The type and geometry of these fractures are determined by stress state. At the same time they determine the macrofracture mode. The more concentration of the axial (tensile) microfractures during the tensile macrofracture forming results more velocity $V^{\perp}$ variations than during the shear macrofracture forming.

Geophysical study of macrofracture forming based on large-scale tests

The present study aim was to explore the 2D regularities of the macrofracture forming in large rock blocks in situ using ultrasonic (US) and acoustic emission (AE) methods. The scheme of the concrete stamp (by size of 1×1 m^2 in plane) shear on rock foundation was selected for the tests [36].

Loading scheme

The study was carried out in situ within the test underground cameras with 3×3 m^2 section. The rock mass is composed of the effusive rocks which are represented by the clastolavas of basalt porphyrites and their lava breccias. The rocks are discontinued by the joints system which form the blocks of different orders starting from 0.15–0.20 m. No anisotropy of the elastic properties was found.

The measurements were carried out using ultrasonic profiling within boreholes [37]. The 7-element ultrasonic probes with distance between sensors of 0.1 m were fixed

within observation boreholes, which after mounting were filled with clay. The measurement lay-outs are represented on Fig. 8a.

The concrete stamp (1) mounted on rock foundation was loaded by the shear load T applied to the front plane (1a) and normal load N applied to stamp top. The normal load was increased from zero up to N value which was kept constant during loading test. The shear load was increase by steps ΔT from zero up to ultimate value Ts. The ultrasonic probes (2) were located within drill holes (2) in central vertical stamp plane. One of zondes was always located near the front plane and the second one near the back plane (1b). Third probe was used for ultrasonic tomography between drill holes. Such scheme permitted studying of the macrofracture forming zones at all loading level.

After T load increasing the displacements increased during 10–15 min up to stable value and velocity of the longitudinal (Vp) and transversal (Vs) waves were measured within 10 cm zonde intervals and along all possible tomography rays (12). The acoustic emission sensor (4) was located within short drill hole near the front or back planes as well as at the stamp center for studying of the local microseismic activity.

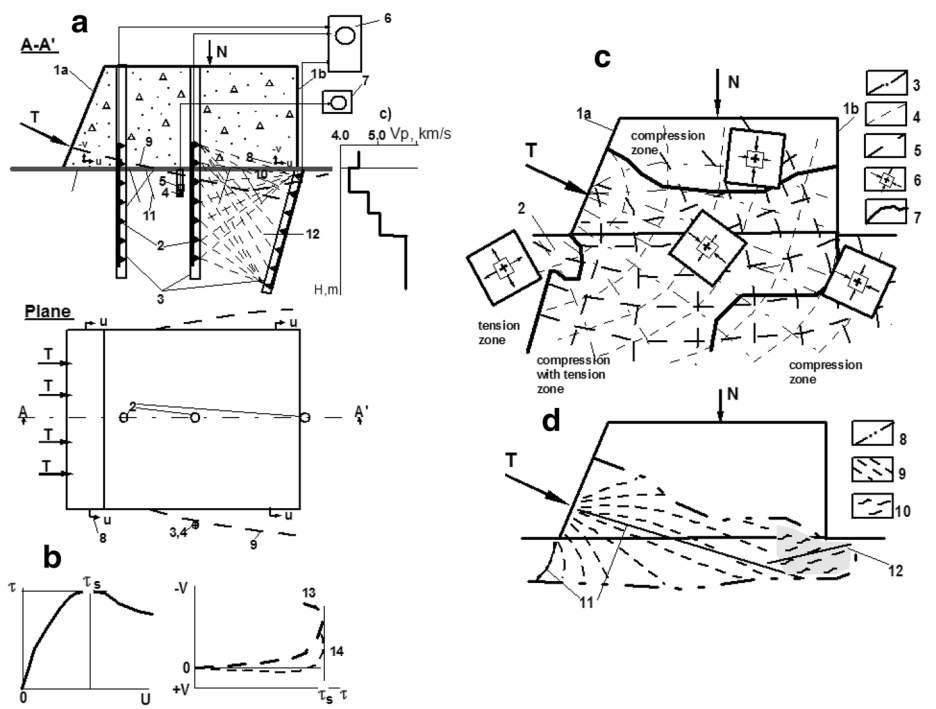

Fig. 8 **a** Seismic-acoustic measurement layouts in section and in plane; **b** displacement graphs under front (loaded) plane of the concrete stamp and back planes (*1b*); **c** typical velocity Vp graph in rock foundation; **d** Stress field; and **e** plastic deformation area at the section of the 'stamp-rock' system at the load level of 0.85 from strength. In **a**–**c** *1a* and *1b*—front and back plains of stamp, *2* ultrasonic zonde, *3* drill holes, *4* AE sensor, *5* preamplifier, *6* US scope, *7* magnetic tape, *8* displacement meter, *9* tensile macrofracture, *10* shear macrofracture, *11* natural joints, *12* tomography rays, *13,14* vertical displacement vs loading level graphs of the front and back planes, accordingly; In (**e**) and (**d**) *1a*, 1*b* the same as in a, *2* rock foundation, *3–5* traces of the main stresses σ_1, σ_3 and τ_{max}, accordingly. *6* stress state mode, *7* boundary of the different stress state mode zones, *8* plastic zone boundary, *9*, *10* rupture and shear microfractures, accordingly, *11*, *12* tensile and shear macrofractures, accordingly

Failure mechanism of the "stamp-foundation" system

The failure of 'stamp-rock foundation' system is take place by tensile fracture at the front stamp plane and shear fracture or crushing (in the strongly heterogeneous rock) at the back one. In first case the angle between displacement vector and fracture plane is 60°–90° and in second case it is 30°–45°. The foundation is stiffer the rupture under front plane is more clearly expressed. The typical macrofracture mode is represented in Fig. 8a. The failure starts at the front (loaded) plane: the rupture fracture (9) is extended under the back plane. The final failure takes place along shear fracture (10) at the back plane. The stress state at the 'stamp-rock foundation' system is shown in Fig. 8d. The calculations shown that under the front plane the "pressure–tension" stress zone and under the back plane the "pressure–pressure" stress zone are formed at the first load steps. In accordance with Mohr criterion [24] the plastic zone is formed at the front plane and extended under back plane. At the loading level of 0.85 from strength the plastic zone occupies the all contact zone (Fig. 8e). At that the microfractures of the rupture mode are formed within almost all contact area apart from small zone located near the back plane where shear microfractures are formed.

Velocity behavior within macrofracture forming zone during stamp loading up to failure

Velocity dimensional behavior in macrofracture forming zone of different mode

The dimensional velocity variation at different removal from tensile and shear macrofracture are shown in Fig. 9.

The dependences for medium foundation stiffness are analyzed (elastic modulus ratio Econcrete/Erock =1.5). The rupture zone is characterized by the gradual velocity decrease (Fig. 9a) at all loading stages. The decrease amplitude (δV% < 0) is maximum

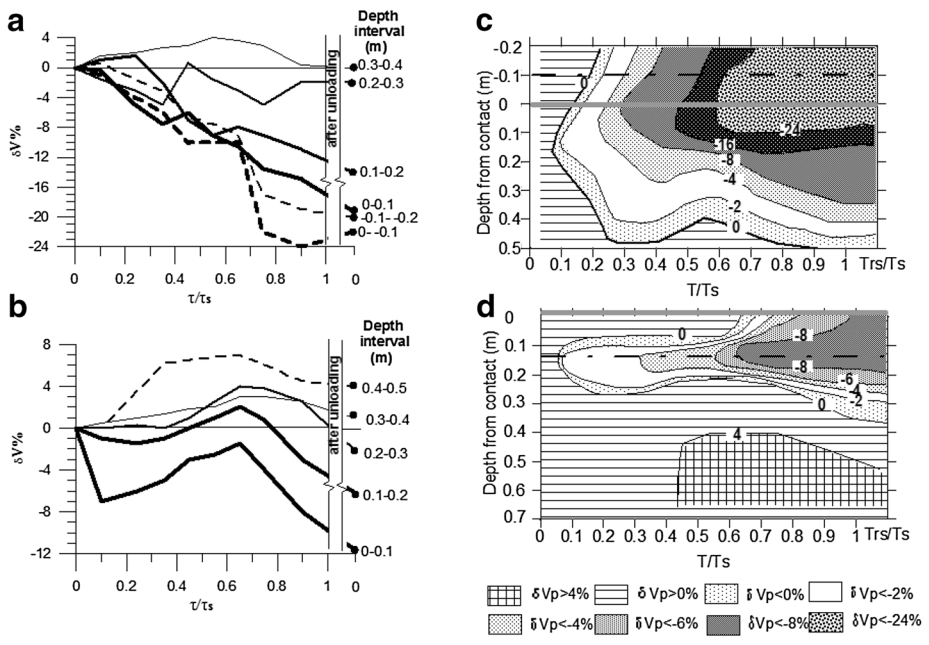

Fig. 9 **a** Relative interval velocity variations δV% vs relative shear stress τ/τs graphs at the rupture; and **b** Shear fracture zones; **c**, **d** distribution of the δV% in the stamp-rock section at the different loading levels in rupture zone (loaded stamp side) (**c**) and shear one (**d**)

close to macrofracture position (−24 to −30%) and it decreases as distance from macrofracture increases (to −4%). In distance of 0.3–0.4 m velocity (δV %) changes sign to positive.

In shear zone velocity behavior is more complex (Fig. 9b), but in whole, it is quite regular.

The common for all tests is existence of the depth interval (0.1–0.3 m), which demonstrates sharp velocity decrease from first loading steps. This decrease then is changed by the gradual velocity increase. This depth interval is located on continuation of the shear load line and evidently it is connected with features of the loading geometry. Other regularity is a common velocity increase in all depth intervals up to loading level of 0.65–0.80 from strength. Then velocity decrease starts and it is continued to system failure. Above mentioned is clearly seen at the 2D presentation shown in Fig. 9c, d. It is seen from Fig. 9c that at the first loading steps the velocity variation field is formed and its image doesn't change in following stages but the velocity variation amplitude is changed only.

The velocity variations depend on stamp-rock stiffness ratio. As rock stiffness increases the velocity behavior is more complex, especially in shear fracture forming zone. But in all cases the system failure took place at the background of the velocity decrease. This decrease started at the lower load level (0.65–0.8 from ultimate load) for weaker rocks and at the load level of 0.9 and more for stiff rock foundation. The summary velocity decrease in shear zone before the system failure was −8 to −12% in average (Fig. 9d).

So, character of the velocity behavior is defined by the macrofracture mode that in his turn is defined by stress mode. The velocity variation amplitude depends on stress-state mode, normal stress level and the primary (before loading) rock elastic properties.

Active zone

Analysis of the velocity behavior at the different distances from macrofracture zone shown that it is complex and it is difficult to define the deformation stage using interval velocity only. The above results show that in real rock mass the main deformations are localized within zone (named active zone), which is characterized by heightened velocity and geomechanic parameter variations. It could be supposed that integral characters of this zone have to reflect deformation process, which is not homogeneous within this zone. It was established using statistical analysis that the active zone sizes in rupture zone is 0.3–0.4 m (or 30–40% of the stamp size) and in shear zone it is 0.5 m (or 50% of the stamp size).

In Fig. 10a active zone velocities variations are represent as against loading level. One can see that active zone integral velocity graphs are similar to generalized velocity behavior during the deformation process preceding to tensile (a) and shear (b) failure. Moreover, maximum correlation between strength and velocity takes place when velocity of the active zone is used.

Repeated loading of the system

The velocity variation difference in the tensile and shear failure zones is interpreted in terms of the microfractures accumulation and interaction. The first, conditions for microfractures forming are confirmed by calculations using Mohr criterion. It is evidently that there is a difference in velocity behavior within tensile and shear failure

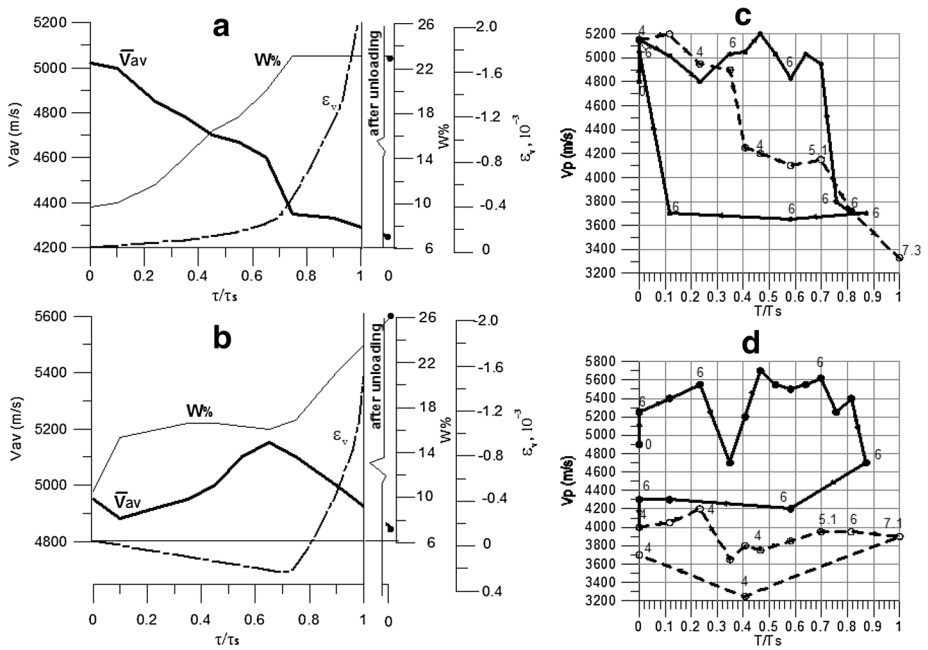

Fig. 10 Variations with loading level of the active zone velocity Vav, variation coefficient W% and summary active zone vertical deformation εv in the tensile (**a**) and shear (**b**) failure zone; (**c**) Active zone velocity vs loading level graphs in the tensile (**c**) and shear (**d**) failure zones at the repeated loading (digits are normal effective stress)

zones. We will consider the repeated loading of the stamp-rock system firstly loaded to loading level of 0.85 (Fig. 10c, d). The stamp is loaded by the shear load T (at the normal stress of 6 MPa) up to T/Ts = 0.85. At that velocities in rupture zone decrease from 5200 to 3600 m/s and in shear failure zone from 5250 to 4380 m/s. The unloading of the system leads to restoration of the velocity in rupture zone and following velocity decrease to 3800 m/s in shear failure zone. During repeated loading of the stamp (at the normal stress of 4 MPa) velocities within rupture zone decrease from 5200 to 3250 m/s. At the loading level of 0.85 normal stress is increased to 6 MPa and velocity is restored to its value in the first loading at the same normal load. The velocity in the shear failure zone during repeated loading are varied at the considerably low level. So, velocity variations in the rupture failure zone are convertible and in the shear failure zone they are nonconvertible. It means from our point of view that in rupture failure zone the rupture microfractures are formed which can completely close after unloading the system. In the shear failure zone shear mode microfractures are formed which can't restore shape because the friction. The interaction between these fractures evidently takes place that also counteracts to microfractures closing and velocity restoration.

Common regularities of velocity variations during rock deforming

Specific features of this study is a selection of the observation technique which allows velocity measuring along minimum normal stress direction. The samples failure numerous studies have shown that this measurement direction is more informative at the inelastic deformation and failure stage. In all testes, the "stamp-rock" system failure took place at the velocity decrease connected with microfractures forming. Somewhat

velocity conversion took place after system failure at the removal of 0.3–0.4 m from macrofracture for both tensile and shear zones. Evidently, macrofracture forming results the rock unloading and microfractures closing out of the failure zone. The results show that within failure forming zone the complex velocity variations takes place (especially in the stiff rock). It connects with a heterogeneous rock structure, loading geometry as well as stress redistribution after local fracture forming within deformed volume. At the same time velocities measured in the active zone clearly reflects the deformation process stages and its difference within rupture and shear failure zone. The material compaction is accompanied by the velocity dispersion decrease. Contrary, the material failure, microfractures forming leads to velocity decrease and velocity dispersion within failure zone increase. Analogues results were obtained in the Inguri Dam long-term monitoring [9]. It was established that most adequate rock mass deformations of the dam foundation are reflected using integral velocities variations, measured within active zone.

Case histories

The machine hall (MH) of the Hoabinh project is of an underground construction in effusive rocks, by the design the MH is unique construction of 260 m long, 20 m width and 57 m height from the bottom of cavern up to the arc portion. Structures of the power waterway are located in the minimum faulted tectonic block composed mainly of clastolavas of basalt porphyrites and lava breccias formed by clastolavas and lavaclastites. The distinguishing features of construction the MH complicating the process are the following: distinctive characteristics of the design (large chamber excavation located nearby—machine and transformer halls), complicated engineering-geological conditions (shear-risk dikes steeply dipping towards excavations and tectonic fractures of order—V), employment of explosion mass up to 2000 kg and intensive mining operations resulting in a rapid exposure of large areas of the MH walls favoring an embrittle-blocky de-stressing of the rock mass. The most unfavorable combinations of the above mentioned factors is observed in the inter-chamber pillar (ICP) between the machine and transformer halls (TH). At the initial stage the MH construction was accompanied by an intensive large-block inrush of rocks occurring on dipping surfaces of the V-order fractures. In this situation the underground opening construction need the monitoring of the stability of the MH walls especially at the ICP sector. In the first stage of construction numerous ultrasonic survey in the anchor drill holes as well as seismic refraction and tomography in the walls were performed. Statistical presentation about forming and structure of the unloading zones was got. Later in the course of the MH excavation a monitoring network was performed which includes: engineering-geological, geophysical (ultrasonic, acoustic-emission and vibration) dynamo-deformometric observations. It gave a chance to observe in the time the unloading zones development connected with the construction works [11, 15]. In this work the main attention is spared to analysis of the ICP deformation development based on geophysical monitoring.

The rock mass stress-state in the vicinity of machine hall

The natural rock mass stress-state at the MH vicinity was studied using the unloading deformation measurements at the small experimental cameras of the 2.5×2.5 m^2 cross-section. The values and orientations of the main stress tensor components was

determined. They are: vertical stress component $\sigma_v = 6.0$ MPa and horizontal one $\sigma_h = 2.0$ MPa. The stress state calculations based on this estimates were carried out and local rock mass strength around MH were calculated. It was obtained that in the MH walls the over breaking deformation zone is formed in which the local strength criterion is surpassed (Fig. 11). This zone in the upper wall has limited size, but in the lower wall it occupies the whole inter-chamber pillar. In zones, situated near the lower the MH corner the stress state of volumetric compression is formed. In accordance with such stress distribution the project foresees the strengthening of the upper wall using of the 12 m long passive bolt anchor. The lower wall has to be supported using the through cable pre-stress anchors of high bearing capacity (24 m long) over the whole ICP width.

Ultrasonic monitoring of rock mass unloading

The ultrasonic monitoring within ICP was planned for walls stability control. The velocity monitoring was carried out within observation drill holes which was kept during the MH construction period. The velocities were measured in the minimum normal stress direction (in horizontal plane).

In Fig. 11c velocity graphs along drill hole 21-H by observation cycles are shown. In velocity graphs the response of the rock mass to lowering of the MH and TH halls bottom as well as to technogeneous actions is clearly seen: initially it is a uniform velocity graph with a typical low velocity zones near the contour caused by rock failure by blasts (cycle 0), then, it readily responds to the MH bottom moving by forming of three low velocity zones (decompaction in fractures) at intersections of the drill hole with fractures

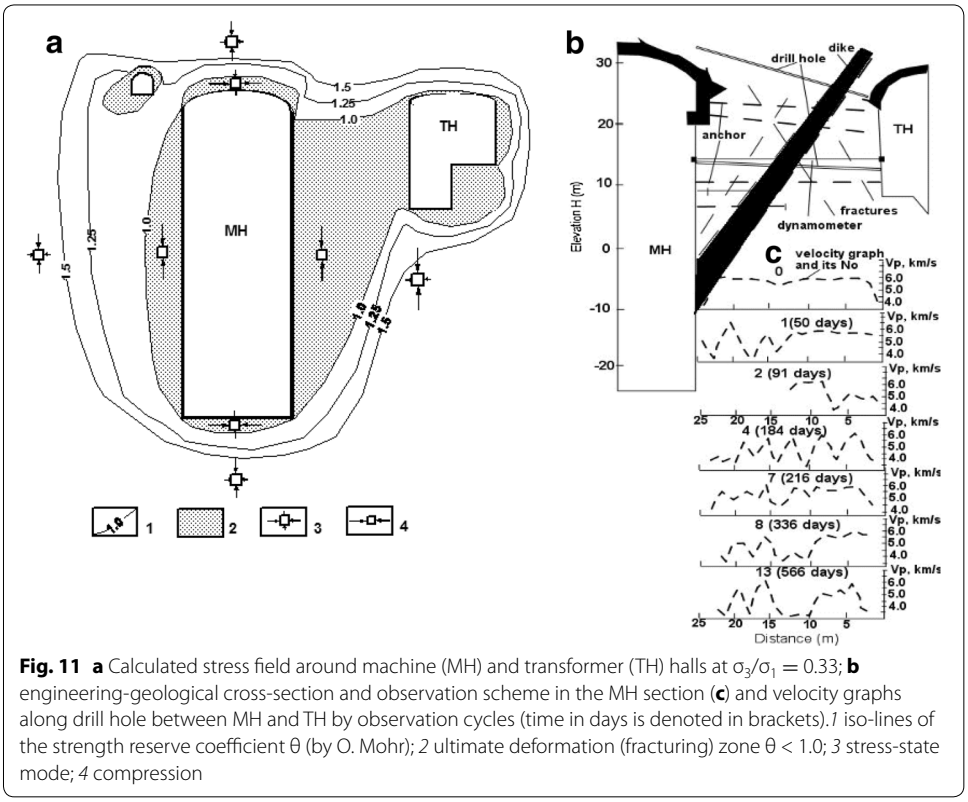

Fig. 11 **a** Calculated stress field around machine (MH) and transformer (TH) halls at $\sigma_3/\sigma_1 = 0.33$; **b** engineering-geological cross-section and observation scheme in the MH section (**c**) and velocity graphs along drill hole between MH and TH by observation cycles (time in days is denoted in brackets).*1* iso-lines of the strength reserve coefficient θ (by O. Mohr); *2* ultimate deformation (fracturing) zone $\theta < 1.0$; *3* stress-state mode; *4* compression

and dykes (cycle 1). It responds to the TH hall bottom lowering also (cycle 2). Gradually low velocity zones are occupies whole ICP (fractures are opened).

The anchor stretching to 100 ton results in gradual velocity increase (compacting of the rock mass through the whole thickness excepting the shear-risk fracture. Such velocity pattern was remained during a some months. In cycle 8 a sharp change of the velocity section was observed by forming and confluence of the low velocity zones at a large depth interval of the drill hole. It took place after excavation of the lower bench by a blast of 600 kg mass. Further velocity decrease connected with a fracture forming of the pillar was continued till cycle 13. Parallel with the change of the velocity structure new fractures were formed on the rock mass surface, new ring fractures were formed in the concrete lining. These processes are shown in Fig. 12 in which an example of the observation data comprehensive presentation is given.

Figure 12a shows the average velocity decrease with time which testify that constant fractures opening through whole inter-chamber pillar takes place. We can see that despite of complex differential patterns of the velocity variations along drill hole connected with fractures opening (Fig. 11c) the velocity measured on all length of borehole shows regular gradual velocity decrease testifying about ICP dilatancy. It is also confirmed by the pre-stress anchors stretch increase (Fig. 12b).

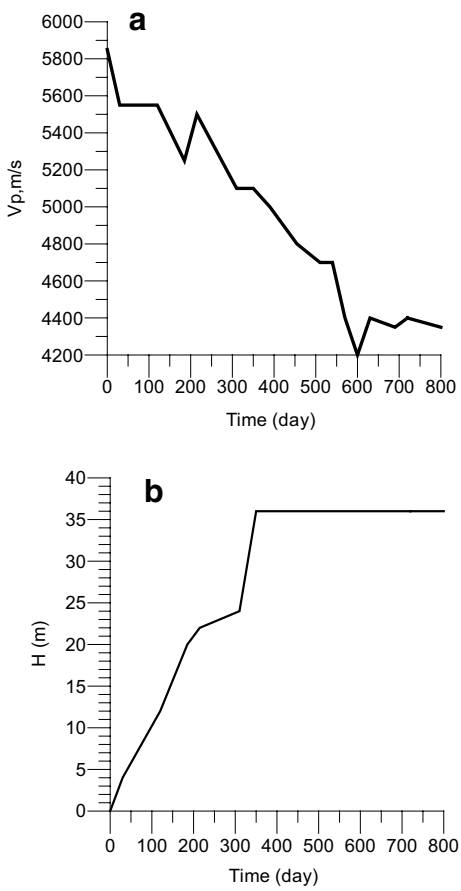

Fig. 12 Average velocity Vp (**a**) and distance of the drill hole to MH bottom (**b**) versus time graphs

Velocity behavior as result of rock mass unloading

At construction of MH and TH the loosed zones are formed in massif, whose dimensions and structure is conditioned by several factors, leading from which is unloading of rocks from natural stresses, redistribution of stresses out of camera contour in process of its excavation. These processes, in different degree develop in any geological conditions and ones most intensively displays in zones of crossing and mutual influence of galleries and cameras. At the quick release of walls and at absence of pioneer support the unloading displays evidently expressed block character, consisting in displacement of large near wall rock blocks into cavity of MH along the surfaces of low orders joints (V or VI). It results the velocity sharp decrease in these fracture zones. Creation of MH cavity causes decrease of radial (horizontal) stress component near the contour. Vertical stress component increases. In massif near the walls and within ICP is formed stress state similar to uniaxial compression. It causes first, opening of large earlier closed cracks with chloritizated filling and cracks or tectonic ruptures with a clay filling followed by breaking or rupture of narrow inter-crack pillars, composed of the chloritizated clastolavas. As result, in rock mass the extension and general number of the potential displacement surfaces increases. The velocity structure has appearance of the alternation of high and low velocity zones (Fig. 13a).

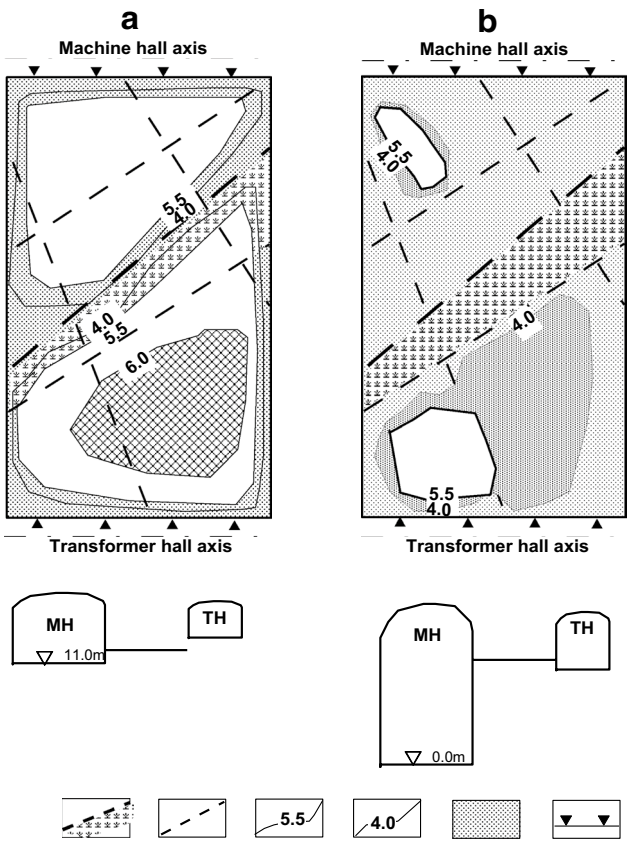

Fig. 13 Velocity map of the rock mass in inter-chamber pillar (map at elevation of 15.0 m) between the bus duct galleries GT-1 and GT-2 at different construction stages: **a** MH *bottom* is at elevation 11.0 m; **b** one at elevation of 0.0 m. 1-V order crack with gabbro-diabase dike; 2-VI order crack; 3-velocity isoline Vp = 5.5 km/s (boundary of loosed zone; 4-one, 4.0 km/s (boundary of the fractured zone); 5-zone of plastic deformation (opened tensile fractures); 6-ultrasonic measurements boreholes

The velocity behavior is affected also by the pre-stress anchors stretching which influences on the stress state and results the velocity variations. The lowering by turns of the MH and TH bottom results the stress redistribution within ICP. Accordingly the velocities of the fractured zones are restored and decreased (Fig. 13b).

Standing of the rock mass in time turns on the reologycal mechanisms: in zones, where stresses are close to rock mass strength, the forming of the small cracks is began. It is appeared in velocity decrease within inter-joint blocks.

Conclusion

The examples described above point to great potentialities of the geophysical methods for rock deformation monitoring. The velocity measurements added by the deformations measurements allows understanding of the fracture parameters variations in both space and time. At that very important factor is a measurement configuration. The velocity measurement along the major stress directions gives different information at different deformation stages. The active zone as a zone of the heightened deformation variation is second very important factor for monitoring of deformation process.

Acknowledgements
This work was made possible through support provided by the Designing and Research Institute Hydroproject, 'named after S.Y. Zhuk' (Moscow, Russian Federation) and Institute of Physic of the Earth by 'named after O.Y. Schmidt' of Russian Academy of Sciences. We thank G.A. Sobolev, A.I. Savich, S.I. Skiba, A.D. Michailov for assistance and fruitful cooperation. We are grateful to many others supported our in situ and laboratory studies.

Competing interests
The author declares that he has no competing interests.

Publisher's Note

Received: 28 June 2015 Accepted: 28 June 2017
Published online: 12 July 2017

References

1. Da Gama CD (2004) A method for continuous monitoring of tunnel deformations during construction and service phases. EUROCK'2004, Salzburg, Austria. http://cegeo.ist.utl.pt/html/investiga/met.pdf
2. Drescher K, Handley MF (2003) Aspects of time-dependent deformation in hard rock at great depth. J South Afr Inst Min Metall 103(5):325–335. https://www.saimm.co.za/Journal/v103n05p325.pdf
3. Jaeger JC, Cook NGW, Zimmerman R (2007) Fundamentals of rock mechanics, 4th edn. Wiley-Blackwell, Hoboken, New Jersey. http://eu.wiley.com/WileyCDA/WileyTitle/productCd-0632057599.html#see-less-auth. ISBN 978-0-632-05759-7
4. Maghsoudi A, Kalantari B (2014) Monitoring instrumentation in underground structures. Open J Civ Eng 2014(4):135–146. doi:10.4236/ojce.2014.42012
5. Roberts L, Mellegard K, Hansen F (eds) (2015) The mechanical behavior of salt VIII, Rapid City, South Dakota, USA. 26–28 May 2015, 137–144. CRC Press, London, ISBN: 978-1-138-02840-1. https://doi.org/10.1201/b18393-18
6. Zienkiewicz OC (1968) Continuum mechanics as an approach to rock mass problems. In: Stagg KS, Zienkewicz OC (eds) Rock mechanics in engineering practice. Wiley, London, pp 237–273
7. Zienkiewicz OC, Taylor RL, Fox D (2014) The finite element method for solid and structural mechanics, 7th edn. Butterworth Heinemann, Elsevier, Oxford. ISBN 978-1856176347
8. Savich AI, Kujundjich BD (eds) (1990) Complex engineering-geophysical explorations at the hydrotechnical construction. Nedra, Moscow **(in Russian)**
9. Savich AI, Ilyin MM, Ezersky MG, Kalinin NI (1983) Long-term geophysical observations on the Inguri dam rock foundation. Bull Int Assoc Eng Geol 26–27:315–319
10. Acrimony JA, Larsson J, Reveler R, Colin P (1987) Displacement remote monitoring and seismic acoustics: what is best fitted to the monitoring of rock caverns. Proceedings of the ISRM International Symposium, Helsinky, 1986. Balkema, Rotterdam, pp 885–900

11. Ezersky MG, Ilyin MM, Yakovlev BP, Kolichko AV (1991) Specific of rock mass unloading during construction of the Rogun hydropower station with the use of geophysical data. Proceedings of the 7th ISRM international congress. Aachen/Deutschland/1991, pp 1099–1104
12. Philips J, Plenkers K, Gartner G, Teichmann L (2015) On the potential of in situ acoustic emission (AE) technology for the monitoring of dynamic processes in salt mines. In: Roberts L, Mellegard K, Hansen F (eds) The mechanical behavior of salt VIII. Rapid City, South Dakota, USA. 26–28 May 2015, 89–98. CRC Press, London, ISBN: 978-1-138-02840-1
13. Ezersky MG, Skiba SI, Mikhailov AD (1993) Geological geophysical monitoring of stability of the underground power house of Hoabinh Project (Vietnam) during construction. In: Proceedings of ISRM International Symposium/1993.06, 21–24, "Eurock'93"/Lisboa/Portugal. International Society for Rock Mechanics, Balkema, Rotterdam, pp 535–544 (**was published also in the Journal Hydrotechnicheskoe Stroitelstvo. 1990 No. 5, p.34-36 (in Russian)**)
14. Yu X, da Gama CD, Na Y, Wang Q, Xie Q (2005) Deformation behaviour of rocks under compression and direct tension. J South Afr Inst Min Metall 105(1):55–62
15. Ezersky MG, Rudijak MS, Zhdanov VV (1993) Forecast and stability monitoring of Zhinvali project tunnel on basis geophysical data. Proceedings of the ISRM international symposium Istanbul/Turkey/5-7 April 1993. A. A. Balkema, Rotterdam, Brookfield, pp 485–491
16. Luth S, Bohlen T, Giese R, Heider S, Hock S, Jetchny S, Polom U, Wadas S, Rechlin A (2014) Seismic tomography and monitoring in underground structures: developments in the Freiberg Reiche Zeche underground lab (Freiberg, Germany) and their application in underground construction (SOUND). In: Weber M, Munich U (eds) Tomography of the Earth's crust: from geophysical sounding to real-time monitoring: GEOTECHNOLOGIEN science report No. 21. Springer International Publishing, Switzerland, pp 115–134. Doi: 10.1007/978-3-319-04205-3_7
17. Ezersky MG, Goretsky I (2015) The scale effect of Dead Sea salt velocities based on seismic-acoustic measurements. In: Roberts L, Mellegard K, Hansen F (eds) Mechanical behavior of salt VIII. CRC Press, Boca Raton, pp 137–144. ISBN: 978-1-138-02840-1. https://doi.org/10.1201/b18393
18. Brace WF, Poulding BW, Scholz C (1966) Dilatancy in the fracture of crystalline rock. J Geophys Res 7(16):3939–3953
19. Kuster GT, Toksöz MN (1974) Velocity and attenuation of seismic waves in two-phase media. Part I. theoretical formulations. Geophysics 39(5):587–606
20. Salganik RL (1979) Mechanics of bodies with many cracks. Mech Solids 8:35–143 **(English Translation)**
21. Scholz CN (1968) Microfracturing and the inelastic deformation of rock in compression. J Geophys Res 73(4):1417–1432
22. Spies T, Hesser J, Eisenblatter J, Eilers G (2005) Measurement of acoustic emission during backfilling of large excavations. In: Potvin Y, Hudima M, (eds) Proceedings of the 6th Symposium Rockbursts and seismicity in mines (RaSiM 6). Australian centre for geomechanics Australia, pp 379–383
23. Muller L (1963) Der Felsbau, Salzburg Erster Band. Teoretischer Teel: Ferdinand Enke Verlag Stutgart
24. Hoek E (1968) Brittle failure of rock. In: Stagg KS, Zienkevich OC (eds) Rock mechanics in engineering practice. Wiley, London, pp 99–124
25. Brady BT (1974) Theory of earthquakes, 1. A scale independent theory of rock failure. Pure Appl Geophys 112:701
26. Stavrogin AN, Protosenya AG (1983) Rock plasticity in conditions of variable deformation rates. J Min Sci 19(4):245–255
27. O'Connel RJ, Budiansky B (1974) Seismic velocities in dry and saturated cracked solids. J Geophys Res 79(35):5412–5426
28. Ezersky MG (1985) Seismic-acoustic parameters behavior preceding to samples and rock mass failure. Ph.D. thesis, Moscow institute of the physics of earth of the Russian academy of sciences. (in Russian)
29. Crampin S, McGonigle R, Bamford D (1980) Estimating crack parameters from observations of P-wave velocity anisotropy. Geophysics 45(3):345–360
30. ASTM, Standard D 2845 (2005) Standard test method for laboratory determination of pulse velocities and ultrasonic elastic constants of rock. ASTM International, West Conshohocken, PA. doi:10.1520/D2845-05. www.astm.org
31. Terentiev VA (1993) Compact field impulsive ultrasonic meter S-70. USSR Acad Sci Izv Phys Earth Ser 11:54–57
32. Rao MVMS, Lakshmi KJP (2003) Shear-wave propagation in rocks and other lossy media: an experimental study. Curr Sci 85(8):1221–1225
33. Beck AE (1981) Physical principles of exploration methods. Macmillan Press Ltd., London
34. Savich AI, Koptev VI, Nikitin BN, Yaschenko ZG (1969) Seismic-acoustic methods for study of the rock masses. Nedra Publishers, Moscow **(in Russian)**
35. Pacher F (1970) Deformability of rock masses: mechanism and character of deformations. Effect of loading and time. Proceedings of the 2nd ISRM Congress, Beograd, vol 4, pp 213–219
36. Fishman YA, Gaziev EG (1974) In-situ and model studies of rock foundation failure in concrete blocks shear tests. Proceedings of the 3rd congress of ISRM, Denver, 1974
37. Ezersky MG, Goretsky I (2014) Velocity-resistivity versus porosity-permeability inter-relations in Dead Sea salt samples. Eng Geol 184:96–115. doi:10.1016/j.enggeo.2014.09.009